How Correlated is the $FeSe/SrTiO_3$ System?

Subhasish Mandal,[1] Peng Zhang,[2,*] Sohrab Ismail-Beigi,[1] and K. Haule[3]
[1]Department of Applied Physics, Yale University, New Haven, Connecticut 06511, USA
[2]Department of Physics, Xi'An Jiaotong University, Xi'an, Shaanxi 710049, People's Republic of China
[3]Department of Physics, Rutgers University, Piscataway, New Jersey 08854, USA
(Received 21 September 2016; revised manuscript received 9 April 2017; published 8 August 2017)

Recent observation of ~10 times higher critical temperature in a FeSe monolayer compared with its bulk phase has drawn a great deal of attention because the electronic structure in the monolayer phase appears to be different than bulk FeSe. Using a combination of density functional theory and dynamical mean field theory, we find electronic correlations have important effects on the predicted atomic-scale geometry and the electronic structure of the monolayer FeSe on $SrTiO_3$. The electronic correlations are dominantly controlled by the Se-Fe-Se angle either in the bulk phase or the monolayer phase. But the angle sensitivity increases and the orbital differentiation decreases in the monolayer phase compared to the bulk phase. The correlations are more dependent on Hund's J than Hubbard U. The observed orbital selective incoherence to coherence crossover with temperature confirms the Hund's metallic nature of the monolayer FeSe. We also find electron doping by oxygen vacancies in $SrTiO_3$ increases the correlation strength, especially in the d_{xy} orbital by reducing the Se-Fe-Se angle.

DOI: 10.1103/PhysRevLett.119.067004

Introduction.—In addition to the cuprates, the discovery of superconductivity in Fe-based compounds with superconducting critical temperatures (T_c) ranging from 26 to 56 K has created a new class of unconventional superconductors [1–3]. Recent observations of T_c reaching as high as 100 K in a FeSe monolayer grown on $SrTiO_3$ (STO) have further boosted interest to search for high T_c superconductors in this family [4–11]. Photoelectron spectroscopy measurements show that, unlike other Fe-based superconductors, the Fermi surface of single-layer (one unit-cell) FeSe on STO consists only of electron pockets at the zone corners (X point), without the hole pockets around the zone center (Γ point) [11–14]. This can lead to a different mechanism of gap opening other than the sign changing s-wave pairing state from spin fluctuation found in Fe-based superconductors in its bulk phase [15]. Apart from the Fermi surface, there are many contrasting signatures observed in the monolayer phase of FeSe when compared to the bulk pnictides. For example, the FeSe/STO system was suggested to be in close proximity to a Mott-insulating phase where an insulator-superconductor crossover was found. It was then concluded that similar to the cuprates, the correlation strength was found to be controlled by the Hubbard-U interaction [10,14]. A recent study based on density functional theory (DFT) shows antibonding hybridization between Fe- d and Se- p increases in the monolayer and thus can lead to decreased electron correlation through increasing bandwidth [8]. Various experiments also suggest electron doping makes the FeSe/STO system more correlated [10,13,16], opposite of what usually happens in the bulk iron pnictides [17]. More contrasting behavior is noticed where the enhancement in T_c in FeSe/STO was suggested to arise from strong interfacial effect [11–13].

While there are many density functional based studies describing the role of phonons [9,18,19], band structure [8,20–22], and the epitaxial growth of FeSe/STO [20,22], so far there is no direct explanation of why FeSe/STO behaves so dramatically different than its bulk phase [23] using a method that truly captures fluctuating local moments. Using DFT in combination with the dynamical mean field theory (DFT+DMFT) method [24,25] we study four phases of FeSe and STO: (I) FeSe bulk, (II) a freestanding FeSe monolayer, (III) FeSe on a $SrTiO_3$ substrate without oxygen vacancies (FeSe/STO), and (IV) FeSe on $SrTiO_3$ substrate with 50% oxygen vacancies (FeSe/STO-Ovac) since oxygen vacancies can be a potential source of electron doping as observed in recent experiments and theory [13,20–22,26]. In addition, we study a freestanding FeSe monolayer, chopped from an FeSe/STO-Ovac structure maintaining the same Se-Fe-Se angle of FeSe/STO-Ovac to investigate the effect of the substrate. Here we attempt to address the following questions: (i) How do the electron correlations change from the bulk phase to the monolayer phase? Typically going from bulk to two dimensions, electron correlations increase due to the reduction of the electron's hopping in one direction. Is it true for the Fe pnictide? (ii) What is the origin of electron correlations? Hubbard-U or Hund's coupling J or both? (iii) Can electron correlations change the topology of the Fermi surface compared to that obtained in conventional DFT? (iv) Why electron doping through O vacancies in STO increases the correlation in the FeSe monolayer?

Method and structural details.—The pcnitide height and/or bond angle between X-Fe-X (X = pnictide) plays an important role in determining the strength of the

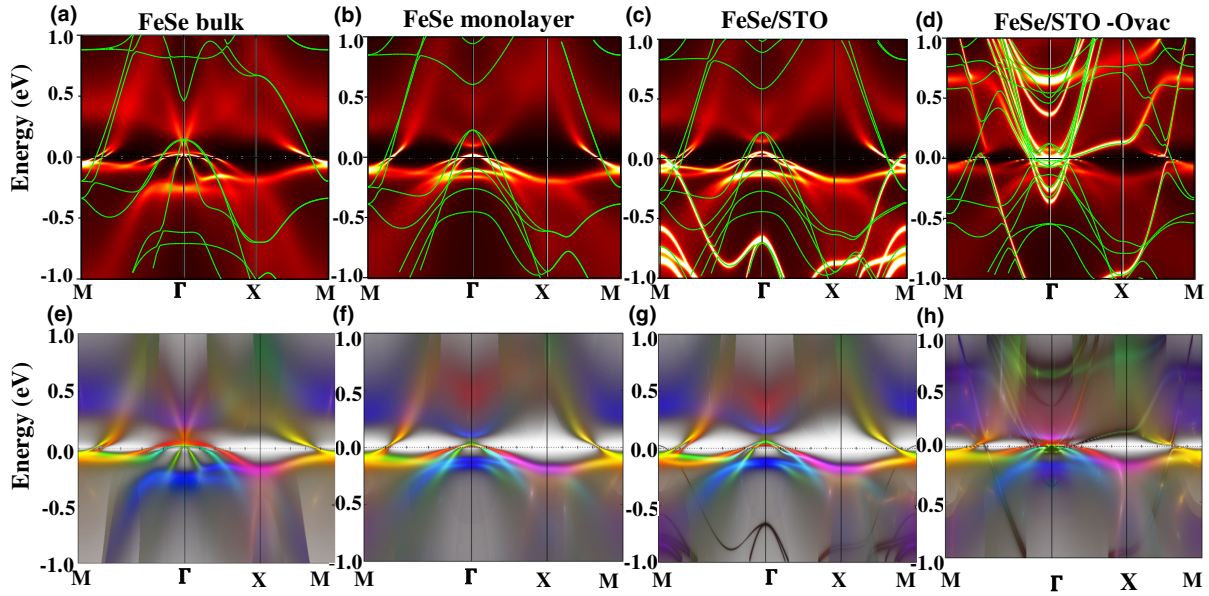

FIG. 1. (a)–(d) Computed DFT+DMFT spectral function together with band structures computed within DFT (green lines) for FeSe bulk (a), FeSe monolayer (b), FeSe/STO (c), and Fe/STO Ovac (d). (e)–(h) Corresponding orbital resolved DFT+DMFT spectral functions: d_{z^2} and $d_{x^2-y^2}$ are in blue, d_{xz} and d_{yz} are in green, d_{xy} is red.

correlations [27,28] and T_c [29] across various compounds in the bulk phase. However, its experimental determination for the monolayer phase is still on going. An accurate determination of the structural parameter is essential due to its extreme sensitivity in controlling the strength of correlation and T_c. In this Letter, relaxed structures are obtained using the self-consistent DFT with embedded DMFT method that incorporates the effect of the electron's entropy while computing forces on atoms. The implementation of the force optimization within DFT+DMFT and the resulting accuracy in obtaining the pnictogen height in bulk FeSe is described in Ref. [30]. To compare the effect of spin fluctuation and electron entropy in the structural optimization, we also obtain atom positions from both nonmagnetic (NM) and spin-polarized (SP) flavors of DFT. More details of our methods and structural information are described in the Supplemental Material [31]. In Table I in the Supplemental Material [31], we describe the key structural parameters. The DFT+DMFT-computed bond angle of Se-Fe-Se in FeSe/STO and the pncitide height (h_{Se}) are closer to the spin-polarized DFT than the nonmagnetic DFT [37]—indicating the local spin fluctuation and the long range order have a similar effect in determining h_{Se} and the angle [30,38]. However DFT+DMFT predicts structures with smaller Se-Fe-Se angle than SP-DFT. Going from bulk FeSe to monolayer, the Se-Fe-Se angle increases from 103° to 109° and h_{Se} is decreased by 7.0% (see the Supplemental Material [31]). With the introduction of oxygen vacancies in STO, the angle reduces to ∼107°. Interestingly the angle in the monolayer phase is close to the "magic" angle where the T_c is found to be the highest in the bulk phase of Fe pnictides [29].

Spectral function.—Once we optimize the atom positions using DFT+DMFT, we compute spectral functions shown in Figs. 1(a)–1(h). Understanding the strength of electron correlations and the nature of the Fermi surfaces are fundamental tasks to understand unconventional superconductivity [39–41]. On the top panels of Figs. 1(a)–1(d), we show DFT+DMFT computed spectral functions on the same color scale for four different systems. The green lines indicate the DFT band structures computed for the SP DFT-optimized structures in the monolayer phase. Brighter color in the spectral function reflects quenched correlation. From bulk to monolayer phases, we notice a significant shrinking in the size of the hole pockets around Γ. This is not prominent in the DFT bands, which reflects the effect of correlation to be important. The increase in the sharpness of the DFT+DMFT spectral function is noticed while going from the bulk phase to the FeSe monolayer and hints that they exhibit a different degree of electron correlation. From bulk to monolayer phases, the DMFT spectral function becomes more coherent—indicating the suppression of correlations in the FeSe monolayer and FeSe/STO. With O vacancies, the spectral function around Γ again becomes dim, which reflects the increase of correlation. We find significant changes in the topology of the Fermi surface in the monolayer phase, especially around the Γ point. The spectral function in the freestanding FeSe monolayer and FeSe/STO are very similar. But introducing O vacancies in STO makes the Fermi surface significantly different.

To identify the orbital dependent nature of the electron correlation effect, we compute DFT+DMFT orbital-dependent spectral functions for the four systems and plot them together on the bottom panel in Figs 1(e)–1(h). The

electron and hole pockets are mainly made of d_{xy} (red) and d_{xz+yz} orbitals (green). Going from bulk to the monolayer phases, the xy pocket around Γ shrinks the most and also changes the sharpness and becomes less correlated in the FeSe monolayer and FeSe/STO and again becomes correlated in FeSe/STO-Ovac. With the introduction of O vacancies in STO, the DMFT spectral function becomes more correlated for all t_{2g} orbitals. Computed DFT+DMFT spectra show that the hole pocket at the Γ point shrinks significantly and almost vanishes when O vacancies are introduced while the electron pockets are found to get bigger. This leads to electron doping similar to Refs. [20–22].

Coherent scale.—In Fermi liquid theory, the inverse quasiparticle lifetime equals to the scattering rate $\Gamma = -Z\mathrm{Im}\Sigma(i0^+)$, where $Z = [1 - \partial\mathrm{Re}\Sigma(\omega)/\partial\omega]|_{\omega\to 0}$ is the spectral weight and $\mathrm{Im}\Sigma(i0^+)$ is the imaginary part of self-energy at zero frequency. At low temperatures when $\mathrm{Im}\Sigma(i0^+) \to 0$, the system is in the coherent phase with infinite quasiparticle lifetime. When the temperature is above the coherent energy scale, $\mathrm{Im}\Sigma(i0^+)$ and, consequently, the quasiparticle lifetimes are both finite. Our DFT+DMFT calculations show that the coherent scales of Fe-3d electrons are strongly orbital dependent (see Supplemental Material [31] for all five d orbitals) and also tuned by the structure of the FeSe/STO system. In Fig. 2(a), the imaginary part of quasiparticle self-energy $\mathrm{Im}\Sigma(i\omega_n)$ of the Fe-3d_{xy} orbital at 150 K are extrapolated to $i0^+$. The extrapolated values are shown in the inset. This directly shows the coherent scales for the four different systems. $\mathrm{Im}\Sigma(i0^+)$ of FeSe bulk and FeSe/STO-Ovac are sizable [see Fig. 2(a) and Fig. S1 of the Supplemental Material [31]] at 150 K, which indicates that the d_{xy} orbital is incoherent and the coherent scales of FeSe/STO-Ovac and bulk FeSe are similar. In contrast, although $\mathrm{Im}\Sigma(i0^+)$ of the FeSe monolayer and FeSe/STO are still finite, their absolute values are much smaller, indicating their coherence at 150 K. The behavior of $\mathrm{Im}\Sigma(i0^+)$ for these four systems at a fixed temperature indicates that the monolayer structure of FeSe and its growth on the STO substrate greatly enhance their corresponding coherent energy scales in t_{2g} orbitals. Dramatically, oxygen vacancies in STO again change the coherent scale in all Fe- d orbitals.

Since the Fermi surface of FeSe/STO-Ovac is the closest to the ARPES measurements, we examine the oxygen vacant FeSe/STO system in more detail. First, we investigate the effect of U and J on Z in FeSe/STO-Ovac. When J is changed from 0.8 to 0.5 eV with a fixed U, the change in Z is found to be stronger than when U is changed from 5.0 to 2.0 eV with a fixed J (Table II in Supplemental Material [31]). This shows the system to be more sensitive to a change in J than U and also confirms the Hund's metallic nature found in bulk pnictides. We also explore the temperature driven coherence-incoherence crossover in FeSe/STO-Ovac. Although it is well known that bulk pnictides are incoherent bad metals [42–45], there is no

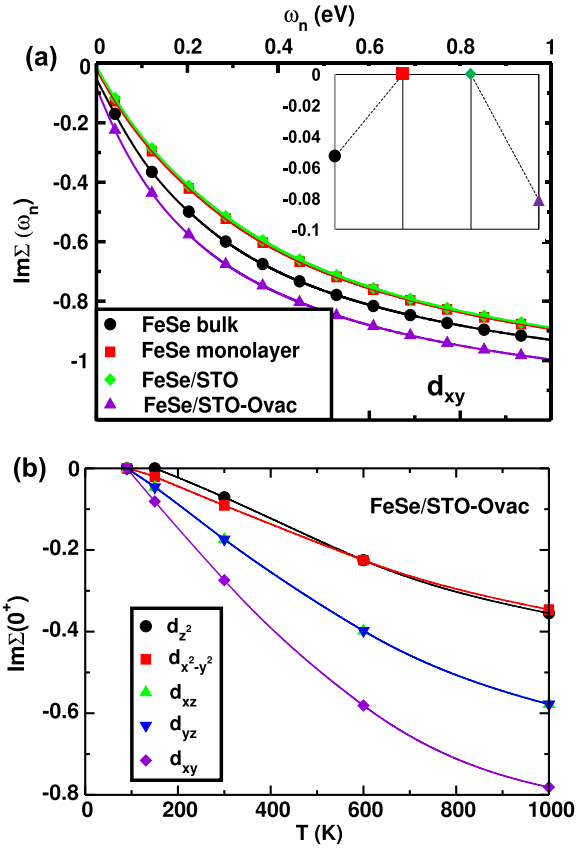

FIG. 2. (a) Imaginary part of self-energy $\mathrm{Im}\Sigma(i\omega_n)$ of the Fe-d_{xy} orbital for four different systems; inset shows the extrapolated value $\mathrm{Im}\Sigma(i\omega_n \to i0^+)$ reflecting structure dependent coherence to incoherence crossover at 150 K. (b) Temperature dependence of $\mathrm{Im}\Sigma(i\omega_n \to i0^+)$ in FeSe/STO-Ovac for the Fe-3d orbitals to show temperature driven coherence-incoherence crossover with orbital dependent crossover temperatures.

study found in the literature for the monolayer phase. A recent study based on the slave-Boson approach showed that the d_{xy} orbital of FeSe/STO behaves like a Mott insulator [10]. We show the temperature dependence of the extrapolated values $\mathrm{Im}\Sigma(i0^+)$ of FeSe/STO-Ovac in Fig. 2(b). At 90 K, all $\mathrm{Im}\Sigma(i0^+)$ are very small, proving FeSe/STO-Ovac is in the coherent state. As temperatures increase from 90 to 1000 K, $\mathrm{Im}\Sigma(i0^+)$ move away from zero to finite values, which signatures a temperature driven coherence-incoherence crossover in FeSe/STO-Ovac. The d_{xy} orbital shows the most temperature dependence.

Quasiparticle weight.—The structural-tuned coherent scales are directly related to the electron correlations. To examine the degree of electron correlations in more detail, we compute the orbital dependent spectral weights Z (inverse of mass enhancement m^*/m_{band}) after analytic continuation of the self-energy by the maximum entropy method [46]. Z is unity in a noncorrelated system, and goes to zero in the strongly correlated limit. We compute Z for all the Fe-3d orbitals of the four different structures

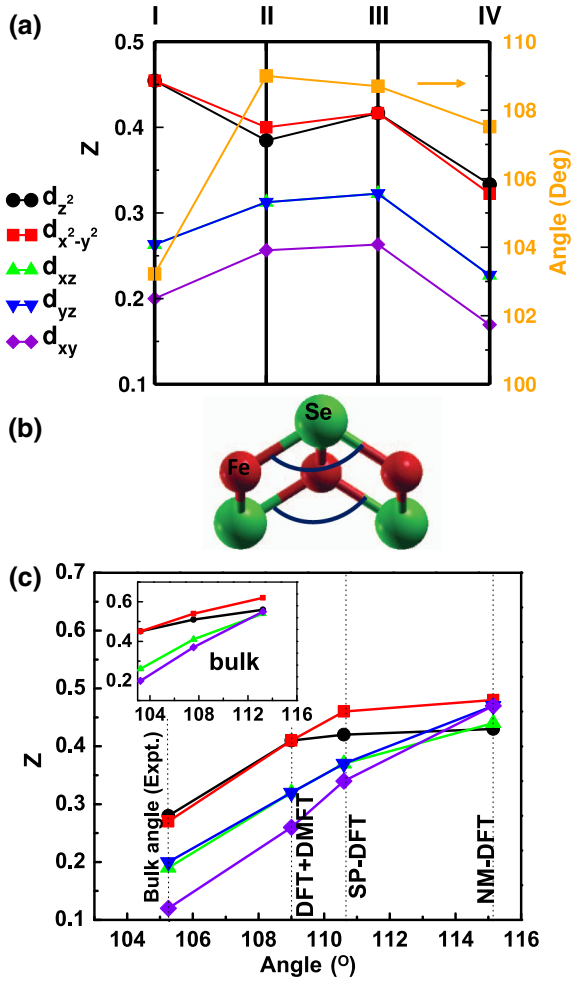

FIG. 3. (a) The spectral weight (Z) on different Fe-3d orbitals (left) and Se-Fe-Se angle (right) show a similar trend across four structures: (I) FeSe bulk, (II) freestanding FeSe monolayer, (III) FeSe/STO, and (IV) FeSe/STO-Ovac. (b) A schematic representation of the Se-Fe-Se angle in FeSe. The angle dependent spectral weights on different Fe-3d orbitals are presented in (c) for the freestanding FeSe monolayer. The dashed lines represent the Se-Fe-Se angle obtained from experiment and optimized with NM-DFT, SP-DFT, and DFT + DMFT methods. Inset represents the angle dependence of Z for bulk FeSe.

[Fig. 3(a)]. First, we notice that the correlation in bulk FeSe has much more orbital differentiation than in the monolayer phase. We find that the d_{xy} orbital is the most kinetically frustrated for both bulk [47] and monolayer phases. Going from bulk to monolayer, all t_{2g} orbitals become less correlated and all e_g orbitals become more correlated. Introducing oxygen vacancies in STO increases correlation in all orbitals. This effect is extremely sensitive in the d_{xy} orbital, which is the most correlated orbital; Z becomes even smaller than in the bulk phase. In FeSe/STO-Ovac, Z in the d_{xy} orbital almost halves, indicating the very strong correlations as observed in the experiment [10,26]. Here, an obvious question arises: why do O vacancies make FeSe/STO so strongly correlated? To answer that, we show the Z as a function of the Se-Fe-Se angle for the four systems [Fig. 3(a)]. Z for all t_{2g} orbitals follow a similar pattern as the Se-Fe-Se angle changes: they first increase from bulk to monolayer and then decrease with the introduction of O vacancies.

In the monolayer phase, the decrease in Z with O vacancies directly relates to the decrease in angle. To prove this, we compute Z as a function of the Se-Fe-Se angle in FeSe monolayers. Figure 3(c) shows a monotonic behavior as we increase the angle.

Three angles are obtained from NM-DFT, SP-DFT, and DFT + DMFT optimization of FeSe monolayers. The fourth angle is for a monolayer structure with Se-Fe-Se angle of bulk. This directly shows that a monolayer structure with the angle of bulk FeSe is extremely correlated and the correlation is controlled by one single structural parameter, which is the Se-Fe-Se angle. We also plot the similar angle dependence of Z in bulk FeSe [Fig. 3(c) inset]. In bulk FeSe, the sensitivity of angle in Z is much less than that in monolayer, especially for the $d_{x^2-y^2}$ and the d_{z^2} orbitals.

Role of oxygen vacancies.—O vacancies serve as a potential source for doping electrons to FeSe as seen in our DFT+DMFT spectral function as well as in the experiments [13,20–22,26,48]. To explore the effect of doping on Z, we construct a monolayer structure with the angle of FeSe/STO-Ovac after chopping out the substrate (FeSe chopped). It is interesting to note that Z in FeSe chopped is slightly lower compared to that of FeSe/STO-Ovac. For FeSe chopped the Z is 0.31, 0.31, 0.22, 0.22, 0.17, while for FeSe/STO-Ovac they are 0.33, 0.32, 0.23, 0.23, 0.17, respectively, for the $d_{x^2-y^2}$, d_{z^2}, d_{xz}, d_{yz}, and d_{xy} orbitals. However the change in Z is not large since a very small amount of charge transfer happens to the Fe-3d orbitals (only 0.02 electron charge transfer is found). It is well known that doping reduces correlation in the bulk pnictides due to weakening of Hund's rule coupling [17]. Our results support this and directly show that it is the reduced angle with O vacancies that increases the correlation. This explains the experimental observation and puzzle of increasing correlation with electron doping in FeSe/STO system via O vacancies. In summary, we show twofold effects of O vacancies: they dope electrons to the FeSe and they increase the correlation because they decrease the Se-Fe-Se angle.

DFT+DMFT hybridization.—The change in the Se-Fe-Se angle can affect the hybridization (or bandwidth). The DFT+DMFT hybridization is shown in Fig. S2 of the Supplemental Material [31]. We notice that the hybridization around the Fermi energy in all t_{2g} orbitals follow a pattern: starting from bulk, it increases for the freestanding FeSe monolayer and FeSe/STO and then again decreases for the FeSe/STO-Ovac. This shows the effect of correlations on the monolayer is directly related to the hybridization modulated by the Se-Fe-Se angle.

Conclusions.—Our results show that the strength of correlations in FeSe/STO heterostructures is dominantly controlled by the Se-Fe-Se angle, which is sensitive to the oxygen vacancies in the STO. The quenched correlations in the freestanding FeSe monolayer and FeSe/STO are directly related to the increased hybridization due to the increase in the Se-Fe-Se angle. Introducing O vacancies in the STO reduces the angle and reduces the hybridization; as a result, the system becomes more strongly correlated. Despite several reports claiming superconductivity in FeSe/STO to be mediated by electron-phonon coupling [12,18,49,50], the strength of electron-phonon coupling in conventional DFT is found to be too low to explain the high T_c [19,49]. The structural-tuned increased electron correlations with oxygen vacancies in STO can enhance the electron-phonon coupling in FeSe/STO similarly to bulk FeSe [38]. Our study favors unconventional superconductivity in FeSe/STO, likely with the orbital antiphase s_{+-} pairing symmetry [51], where the two electron pockets have opposite sign of pairing, as the absence of hole pockets disfavors conventional s_{+-} symmetry.

We acknowledge R. E. Cohen and A. B. Georgescu for helpful discussions. We acknowledge Mark Jarrell and Juana Moreno for their important help. S. M. and P. Z. acknowledge the Carnegie Institution for Science. S. M. and S. I. B. acknowledge support from the NSF SI2-SSI program (Grant No. ACI-1339804). S. I. B. acknowledges partial support from NSF MRSEC DMR-1119826. P. Z. acknowledges support from NSFC-11604255. K. H. acknowledges support from NSF DMR-1405303. Major computations are performed at the 'Supermike' at Louisiana State University. Additional computations are performed at the NERSC supercomputing facility, Carnegie Institution for Science, and Yale University Faculty of Arts and Sciences High Performance Computing Center.

*Corresponding author.
zpantz@xjtu.edu.cn

[1] Y. Kamihara, T. Watanabe, M. Hirano, and H. Hosono, J. Am. Chem. Soc. **130**, 3296 (2008).
[2] I. I. Mazin, Nature (London) **464**, 183 (2010).
[3] X. H. Chen, T. Wu, G. Wu, R. H. Liu, H. Chen, and D. F. Fang, Nature (London) **453**, 761 (2008).
[4] J.-F. Ge, Z.-L. Liu, C. Liu, C.-L. Gao, D. Qian, Q.-K. Xue, Y. Liu, and J.-F. Jia, Nat. Mater. **14**, 285 (2015).
[5] Q.-Y. Wang, Z. Li, W.-H. Zhang, Z.-C. Zhang, J.-S. Zhang, W. Li, H. Ding, Y.-B. Ou, P. Deng, K. Chang, J. Wen, C.-L. Song, K. He, J.-F. Jia, S.-H. Ji, Y.-Y. Wang, L.-L. Wang, X. Chen, X.-C. Ma, and Q.-K. Xue, Chin. Phys. Lett. **29**, 037402 (2012).
[6] Y. Lubashevsky, E. Lahoud, K. Chashka, D. Podolsky, and A. Kanigel, Nat. Phys. **8**, 309 (2012).
[7] M. K. Wu, P. M. Wu, Y. C. Wen, M. J. Wang, P. H. Lin, W. C. Lee, T. K. Chen, and C. C. Chang, J. Phys. D **48**, 323001 (2015).
[8] D. Huang, C.-L. Song, T. A. Webb, S. Fang, C.-Z. Chang, J. S. Moodera, E. Kaxiras, and J. E. Hoffman, Phys. Rev. Lett. **115**, 017002 (2015).
[9] K. W. Kim, A. Pashkin, H. Schfer, M. Beyer, M. Porer, T. Wolf, C. Bernhard, J. Demsar, R. Huber, and A. Leitenstorfer, Nat. Mater. **11**, 497 (2012).
[10] M. Yi, Z.-K. Liu, Y. Zhang, R. Yu, J. X. Zhu, J. J. Lee, R. G. Moore, F. T. Schmitt, W. Li, S. C. Riggs, J. H. Chu, B. Lv, J. Hu, M. Hashimoto, S. K. Mo, Z. Hussain, Z. Q. Mao, C. W. Chu, I. R. Fisher, Q. Si, Z. X. Shen, and D. H. Lu, Nat. Commun. **6**, 7777 (2015).
[11] R. Peng, H. C. Xu, S. Y. Tan, H. Y. Cao, M. Xia, X. P. Shen, Z. C. Huang, C. H. P. Wen, Q. Song, T. Zhang, B. P. Xie, X. G. Gong, and D. L. Feng, Nat. Commun. **5**, 5044 (2014).
[12] J. J. Lee, F. T. Schmitt, R. G. Moore, S. Johnston, Y. T. Cui, W. Li, M. Yi, Z. K. Liu, M. Hashimoto, Y. Zhang, D. H. Lu, T. P. Devereaux, D. H. Lee, and Z. X. Shen, Nature (London) **515**, 245 (2014).
[13] S. Tan, Y. Zhang, M. Xia, Z. Ye, F. Chen, X. Xie, R. Peng, D. Xu, Q. Fan, H. Xu, J. Jiang, T. Zhang, X. Lai, T. Xiang, J. Hu, B. Xie, and D. Feng, Nat. Mater. **12**, 634 (2013).
[14] J. He, X. Liu, W. Zhang, L. Zhao, D. Liu, S. He, D. Mou, F. Li, C. Tang, Z. Li, L. Wang, Y. Peng, Y. Liu, C. Chen, L. Yu, G. Liu, X. Dong, J. Zhang, C. Chen, Z. Xu, X. Chen, X. Ma, Q. Xue, and X. J. Zhou, Proc. Natl. Acad. Sci. U.S.A. **111**, 18501 (2014).
[15] I. I. Mazin, D. J. Singh, M. D. Johannes, and M. H. Du, Phys. Rev. Lett. **101**, 057003 (2008).
[16] J. J. Seo, B. Y. Kim, B. S. Kim, J. K. Jeong, J. M. Ok, J. S. Kim, J. D. Denlinger, S. K. Mo, C. Kim, and Y. K. Kim, Nat. Commun. **7**, 11116 (2016).
[17] M. Wang, C. Zhang, X. Lu, G. Tan, H. Luo, Y. Song, M. Wang, X. Zhang, E. A. Goremychkin, T. G. Perring, T. A. Maier, Z. Yin, K. Haule, G. Kotliar, and P. Dai, Nat. Commun. **4**, 2874 (2013).
[18] S. Coh, M. L. Cohen, and S. G. Louie, New J. Phys. **17**, 073027 (2015).
[19] Y. Wang, A. Linscheid, T. Berlijn, and S. Johnston, Phys. Rev. B **93**, 134513 (2016).
[20] J. Bang, Z. Li, Y. Y. Sun, A. Samanta, Y. Y. Zhang, W. Zhang, L. Wang, X. Chen, X. Ma, Q.-K. Xue, and S. B. Zhang, Phys. Rev. B **87**, 220503 (2013).
[21] K. V. Shanavas and D. J. Singh, Phys. Rev. B **92**, 035144 (2015).
[22] K. Zou, S. Mandal, S. D. Albright, R. Peng, Y. Pu, D. Kumah, C. Lau, G. H. Simon, O. E. Dagdeviren, X. He, I. Božović, U. D. Schwarz, E. I. Altman, D. Feng, F. J. Walker, S. Ismail-Beigi, and C. H. Ahn, Phys. Rev. B **93**, 180506 (2016).
[23] I. A. Nekrasov, N. S. Pavlov, M. V. Sadovskii, and A. A. Slobodchikov, Low Temp. Phys. **42**, 891 (2016).
[24] G. Kotliar, S. Y. Savrasov, K. Haule, V. S. Oudovenko, O. Parcollet, and C. A. Marianetti, Rev. Mod. Phys. **78**, 865 (2006).
[25] K. Haule, C.-H. Yee, and K. Kim, Phys. Rev. B **81**, 195107 (2010).
[26] W. Zhao, M. Li, C.-Z. Chang, J. Jiang, L. Wu, C. Liu, Y. Zhu, J. S. Moodera, and M. H. W. Chan, arXiv:1701.03678.

[27] C. Zhang, L. W. Harriger, Z. Yin, W. Lv, M. Wang, G. Tan, Y. Song, D. L. Abernathy, W. Tian, T. Egami, K. Haule, G. Kotliar, and P. Dai, Phys. Rev. Lett. **112**, 217202 (2014).
[28] F. Essenberger, P. Buczek, A. Ernst, L. Sandratskii, and E. K. U. Gross, Phys. Rev. B **86**, 060412 (2012).
[29] H. Okabe, N. Takeshita, K. Horigane, T. Muranaka, and J. Akimitsu, Phys. Rev. B **81**, 205119 (2010).
[30] K. Haule and G. L. Pascut, Phys. Rev. B **94**, 195146 (2016).
[31] See Supplemental Material at http://link.aps.org/supplemental/10.1103/PhysRevLett.119.067004 for structural details and methods, which include Refs. [17, 32–36].
[32] J. P. Perdew, K. Burke, and M. Ernzerhof, Phys. Rev. Lett. **77**, 3865 (1996).
[33] D. Vanderbilt, Phys. Rev. B **41**, 7892 (1990).
[34] M. Liu, L. W. Harriger, H. Luo, M. Wang, R. A. Ewings, T. Guidi, H. Park, K. Haule, G. Kotliar, S. M. Hayden, and P. Dai, Nat. Phys. **8**, 376 (2012).
[35] P. Blaha, K. Schwarz, G. Madsen, D. Kvasnicka, and J. Luitz, *An Augmented Plane Wave Plus Local Orbitals Program for Calculating Crystal Properties*, edited by K. Schwarz (Vienna University of Technology, Austria, 2001).
[36] A. Kutepov, K. Haule, S. Y. Savrasov, and G. Kotliar, Phys. Rev. B **82**, 045105 (2010).
[37] A. Linscheid, Supercond. Sci. Technol. **29**, 104005 (2016).
[38] S. Mandal, R. E. Cohen, and K. Haule, Phys. Rev. B **89**, 220502 (2014).
[39] A. Damascelli, Z. Hussain, and Z.-X. Shen, Rev. Mod. Phys. **75**, 473 (2003).
[40] M. R. Norman, H. Ding, J. C. Campuzano, T. Takeuchi, M. Randeria, T. Yokoya, T. Takahashi, T. Mochiku, and K. Kadowaki, Phys. Rev. Lett. **79**, 3506 (1997).
[41] P. D. Johnson, T. Valla, A. V. Fedorov, Z. Yusof, B. O. Wells, Q. Li, A. R. Moodenbaugh, G. D. Gu, N. Koshizuka, C. Kendziora, S. Jian, and D. G. Hinks, Phys. Rev. Lett. **87**, 177007 (2001).
[42] K. Haule and G. Kotliar, New J. Phys. **11**, 025021 (2009).
[43] Z. P. Yin, K. Haule, and G. Kotliar, Nat. Phys. **7**, 294 (2011).
[44] L. Craco, M. S. Laad, and S. Leoni, Phys. Rev. B **84**, 224520 (2011).
[45] I. A. Nekrasov, N. S. Pavlov, and M. V. Sadovskii, JETP Lett. **97**, 15 (2013).
[46] M. Jarrell and J. E. Gubernatis, Phys. Rep. **269**, 133 (1996).
[47] Z. P. Yin, K. Haule, and G. Kotliar, Nat. Mater. **10**, 932 (2011).
[48] O. E. Dagdeviren, G. H. Simon, K. Zou, F. J. Walker, C. Ahn, E. I. Altman, and U. D. Schwarz, Phys. Rev. B **93**, 195303 (2016).
[49] B. Li, Z. W. Xing, G. Q. Huang, and D. Y. Xing, J. Appl. Phys. **115**, 193907 (2014).
[50] J. J. Lee, F. T. Schmitt, R. G. Moore, S. Johnston, Y. T. Cui, W. Li, M. Yi, Z. K. Liu, M. Hashimoto, Y. Zhang, D. H. Lu, T. P. Devereaux, D. H. Lee, and Z. X. Shen, Nature (London) **515**, 245 (2014).
[51] Z. P. Yin, K. Haule, and G. Kotliar, Nat. Phys. **10**, 845 (2014).